Combustion and Flame 193 (2018) 306–312

Contents lists available at ScienceDirect

Combustion and Flame

journal homepage: www.elsevier.com/locate/combustflame

Effect of ethanol addition on soot formation in laminar methane diffusion flames at pressures above atmospheric

Elizabeth A. Griffin, Moah Christensen, Ömer L. Gülder*

Institute for Aerospace Studies, University of Toronto, 4925 Dufferin Street, Toronto, Ontario M3H 5T6, Canada

ARTICLE INFO

Article history:
Received 21 January 2018
Revised 1 March 2018
Accepted 1 April 2018

Keywords:
High-pressure soot
Effect of ethanol on soot
Sooting propensity of ethanol
Soot in methane–ethanol flames

ABSTRACT

Influence of ethanol addition on soot production in laminar diffusion flames of methane under elevated pressures was investigated experimentally. A high pressure vessel, equipped with a co-flow laminar diffusion flame burner having a 3 mm fuel nozzle diameter, was used for the soot experiments. The amount of ethanol in methane was 10% based on the total carbon of the fuel stream. Pressure range was from atmospheric to 6 bar. To have measurements to be comparable for the purpose of assessing the pressure dependence, the carbon mass flow rate of the ethanol and methane mixture was kept constant at 0.941 mg/s. Luminescent heights of the flames studied did not vary much with pressure excluding the heights of those at atmospheric pressure. Line-of-sight measurements of soot spectral emission were inverted by an Abel type algorithm, assuming axisymmetric flames, to evaluate variations of radial profiles of temperatures, soot concentrations, and soot yields of neat methane and ethanol-doped methane with pressure. Ethanol-doped methane flames displayed higher soot concentrations than those of neat methane flames at all pressures considered in the study; however, pressure dependence of maximum soot volume fraction is almost the same for both neat methane and ethanol-doped methane. The results showed that the maximum soot volume fractions scale with pressure as P^n, where n decreases from about 2.5 to 1.8, from atmospheric to 6 bar. These exponents are similar to measurements reported previously in the literature for gaseous paraffinic hydrocarbons. Maximum soot yields, on the other hand, are almost the same for both flames at 2 bar, but at 4 and 6 bar pressures ethanol-doped methane flames give higher maximum soot yields than neat methane flames.

1. Introduction

Bioethanol and biodiesel are the two major biofuels which are widely available in the global fuel market. The former is mainly manufactured by the fermentation of starch and sugar containing biomass, and the latter from vegetable oils through transesterification. Ethanol has been recognized for a long time as a hydrocarbon fuel extender and, in some cases, a replacement fuel for ground transportation. Combustion properties of ethanol, such as laminar burning speed and extinction characteristics, have been the subject of several studies within the last several decades, see for example [1–5]. One of the potential benefits of ethanol addition to hydrocarbon fuels has been perceived as a reduction in soot formation in non-premixed (diffusion) combustion systems. Most of the time neat ethanol is thought as a nonsooting fuel when burned at ambient conditions. But at a pressure of 3 bar, isolated ethanol liquid droplets displayed a profusely sooting flame shell under microgaravity [6]. Several studies focussing on the soot reduction potential of ethanol addition to hydrocarbons have yielded sometimes conflicting results.

Influence of adding ethanol to an opposed jet diffusion flame of ethylene in air was studied by McNesby et al. [7] by comparing results from numerical simulations with detailed chemical kinetics to the experimental data. Addition of 8% ethanol to fuel side resulted in an increase of soot production mainly via introduction of methyl radical, which is produced by the pyrolysis of ethanol and reacts with propargyl to produce C_4H_6 leading to increased production of benzene. On the other hand, experiments and numerical simulations on a flat premixed flame, with an equivalence ratio of 2.34, implied that upon addition of ethanol the aromatic species are reduced because of a reduction in available carbon to create soot precursors [8]. McEnally and Pfefferle [9] demonstrated that addition of 10% ethanol to ethylene in a coflow laminar diffusion flame increases the soot production, and they argued that ethanol decomposes to methyl radical favoring the production of propargyl radical, C_3H_3, via addition reactions of C_1+C_2, leading to benzene

* Corresponding author.
E-mail addresses: ogulder@utias.utoronto.ca, flame-utias7@usa.net (Ö.L. Gülder).

https://doi.org/10.1016/j.combustflame.2018.04.001
0010-2180/

formation subsequently through the self reaction of propragyl radicals. Thermal decomposition products of ethylene would not include methyl radical, but most other alkane hydrocarbons produce methyl upon decomposition; therefore the observed increase in soot in ethanol-doped ethylene flames is not expected to happen in alkane flames [9]. A study by Salamaca et al. [10] on the effect of ethanol on soot in opposed jet ethylene–air diffusion flames concluded that up to 20% vol ethanol addition increases soot; higher amounts of ethanol results in a decrease of soot production. The authors argued that ethanol, in amounts less than 20%, increases the fuel reactivity in the pyrolysis region leading to increased radicals enhancing PAH formation and growth.

Maricq [11] and Khosousi et al. [12] studied the influence of ethanol addition to gasoline in coflow laminar diffusion flames and concluded that the soot reduction remains insignificant as long as the ethanol in the blend is less than 50%. It was argued that, when the ethanol in the blend is more than 50%, the observed reduction in soot is due to the reduction in aromatics leading to a decrease in soot inception and PAH condensation [12].

The influence of fuel chemistry on soot formation at atmospheric conditions has been studied extensively, see, e.g. [13,14], resulting in a better understanding of soot processes and development of various soot models. However, combustion based prime movers operate at pressures well above the atmospheric for concerns on the engine size and thermal efficiency. The response of the most combustion events to changes in pressure is not monotonic because of the fact that most flame processes are governed by chemical reactions whose rates are not linear. As a consequence, it is not straightforward to project the atmospheric flame results to the combustion events at elevated pressures with confidence. High pressure studies related to effect of ethanol addition on soot are very limited. Influence of adding ethanol and methanol to benzene on soot formation in shock tube pyrolysis was investigated by Frenklach and Yuan [15]. In a wide temperature range from 1580 to 2395 K and at various alcohol to benzene ratios indicated that ethanol was more effective than methanol in reducing the soot concentrations. A reduction in H atoms and formation of OH radicals, that would attack the soot precursors and soot particles, were argued to be the main culprit in the soot reduction observed by adding alcohols to benzene. It was pointed out that the role of H atoms in reactivating relatively stable aromatics to radicals, which would lead to the increased ring growth processes, was curbed by the removal of H atoms upon alcohol addition. In another shock tube pyrolysis study [16], addition of ethanol to toluene at about 66% vol or higher suppressed soot; lesser amounts of ethanol addition enhanced soot production pointing to a synergistic effect. The authors argued that the synergistic effect is due to acetylene formation during ethanol decomposition offsetting the roles of oxidizing species. Storch et al. [17] compared the soot volume fraction measurements of identical isooctane and ethanol–isooctane blend (20% ethanol by liquid volume) sprays injected in to a combustion vessel at 8 bar, and showed that ethanol blend has a higher sooting tendency than pure isooctane. The authors attributed this to the relatively higher latent heat of ethanol leading to late evaporation.

It is not yet feasible to measure turbulent mixing rates in a spatially and temporally resolved manner in atmospheric turbulent diffusion flames. When the pressure is added as another variable, the situation gets compounded further; soot formation and oxidation rates are altered and mixing rates are modified as a result of changing turbulence field. However, relying on the approximations, like flamelet approaches, the information obtained from laminar flame experiments can be utilized in handling the turbulent flames [18]. Laminar diffusion flame experiments at high pressures have the capability to isolate the chemical effects of pressure changes from the physical effects of turbulence provided that the experiments at various pressures are tractable. It should be noted that the high-pressure laminar diffusion flame studies in tractable flames have been an increasing research effort recently and detailed measurements in tractable flames are available for mostly gaseous fuels, see, e.g. [19–21], however, information on the response of sooting propensity of ethanol and ethanol/hydrocarbon flames to pressure changes is lacking. It would be desirable to have the sensitivity of sooting propensity of ethanol and ethanol–hydrocarbon blends to pressure.

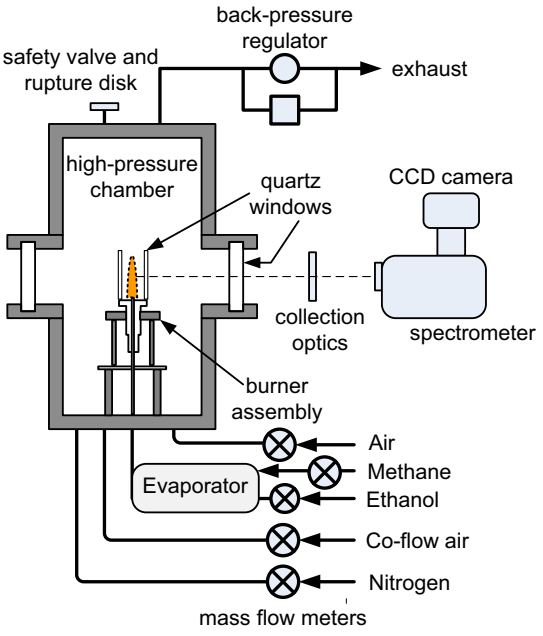

Fig. 1. A schematic diagram showing the main components of the high-pressure experimental rig.

The ultimate aim of the current study is the evaluation of sooting characteristics of laminar diffusion flames of methane and ethanol-doped methane at elevated pressures. Radially resolved temperatures and soot volume fractions were measured up to 6 bar pressure with ethanol-doped methane, and the results are discussed and compared to data from similar flames doped with liquid hydrocarbons.

2. Experimental methodology

A combustion chamber, capable of sustaining pressures up to 110 bar, was used to stabilize the laminar diffusion flames of methane and ethanol-doped methane at pressures from atmospheric to 6 bar. The cylindrical combustion vessel has an internal diamater of 24 cm and a height of 60 cm. It is fitted with three radial observation ports mounted at 0°, 90°, and 180° to provide optical access to the chamber for line-of-sight measurements and 90° imaging and scattering experiments. A 3D translational stage, with a 5 μm movement precision in each direction and controlled by three stepper motors, moves the combustion chamber to the desired measurement location. A circular coflow laminar diffusion flame burner with an exit fuel nozzle diameter of 3 mm and a coflow air nozzle diameter of 25 mm, mounted in the high pressure combustion chamber, was used for the current work, Fig. 1. The stainless steel burner rim is tapered to a fine edge to mitigate the formation of any recirculation zones. Upstream of fuel and air nozzles are fitted with porous metal inserts to provide uniform velocity profiles at the exit of the nozzles. Since extensive details of this rig are documented in the literature before [19,20,22–27], a short account of its main capabilities will be summarized.

Table 1
Mass flow rates of co-flow air and the fuel stream components. f_{lc} = percentage of carbon from ethanol; $\dot{m}_{CH_4}$ = methane mass flow rate; $\dot{m}_{C_2H_5OH}$ = ethanol mass flow rate; $\dot{m}_a$ = co-flow air mass flow rate. The carbon mass flow rate in both flames is kept constant at 0.914 mg/s.

Fuel	f_{lc}	$\dot{m}_{CH_4}$ (mg/s)	$\dot{m}_{C_2H_5OH}$ (mg/s)	$\dot{m}_a$ (mg/s)
CH_4	0	1.221	0	340
CH_4/C_2H_5OH	10	1.099	0.175	340

For the radially resolved temperature measurements in the target flames, we used the soot spectral emission technique as described by Snelling at. al. [28]. Soot volume fractions were inferred from these temperature measurements. For obtaining the temperatures and soot volume fractions in a radially resolved manner in an axisymmetric laminar diffusion flame, the soot spectral emission technique requires information collected at multiple wavelengths [28]. Our current experimental setup includes a spectrometer attached to a calibrated CCD camera for spectral emission measurements. The blackbody radiation from the soot within the flame is collected at the spectrometer after it passes through the collection optics consisting of an adjustable aperture and a lens which focuses the radiation into the spectrometer. Output from the spectrometer is imaged onto the CCD camera as a line-of-sight radiant emission intensities which are binned with 21 nm widths. Spectral radiation data were collected at 100 μm increments in the horizontal direction at a given height and at increments of 1 mm along the vertical flame axis. For a given flame, the whole flame envelope is mapped by recording multiple images with an exposure time of about 1 s. For constructing the radially resolved temperatures and soot volume fractions at 1 mm increments of the height above the burner exit along the flame axis, an inversion algorithm was used to process the spectrally-resolved line-of-sight radiation data. Further details of the temperature and soot volume fraction measurements using the soot spectral emission technique and the inversion algorithm are documented in the literature, see e.g. [25,28,29].

Research grade methane, ethanol, and compressed air were used for the experiments. Methane and compressed air were metered by using mass flow controllers (Brooks SLA5850) which were calibrated for the required mass flow rates using a positive displacement calibration unit (Mesalabs Bios DryCal Definer 220) whose accuracy is traceable to NIST. Ethanol, which was metered by a liquid syringe pump (Teledyne), is fed to an evaporation unit (Bronkhorst) that provides controlled evaporation and flow of gaseous mixtures. The vapourized ethanol mixed with methane is sent to the burner through a heated transfer tube to prevent condensation. The heated fuel transfer tube and the evaporator unit were kept at 200 °C, as well as the co-flow air.

To have measurements comparable at different pressures, the carbon mass flow rates fed into the methane and ethanol-doped methane flames were kept constant. Individual flow rates of ethanol, methane, and co-flow air are listed in Table 1.

Keeping the fuel mass flow rates constant makes sure that the residence times do not change with pressure, and the results can be compared at a given flame height within the flames at different pressures. The assumption here is that the soot data collected at a particular height within the flame at different pressures can be compared to assess the pressure sensitivity. This assumption is based on the experimental and numerical studies which showed that the height of a diffusion flame is not sensitive to pressure if the flow field of the flame is buoyancy dominated . Under buoyancy dominated conditions, residence times are proportional to the square root of the flame height; therefore, equal flame heights mean equal residence times. Experimental observations of laminar diffusion flames at elevated pressures indicate that the cross-sectional area of the flame at various axial heights shows an inverse proportionality to pressure, see, e.g. [20]. With increasing pressure, the mass within the flame envelope is at a higher density, but the flow is through a smaller cross-section. It has been shown that, keeping the mass flow rate of the fuel constant at different pressures, the same centerline velocity along the flame axis is achieved with changing pressure [27,30]. It should be noted that the thermodynamic properties of liquid ethanol and the capabilities of the evaporator unit limited the pressures for this work. The vapour pressure of ethanol and the maximum temperatures the evaporator unit can handle were the major factors on the pressures at which ethanol can be vaporized.

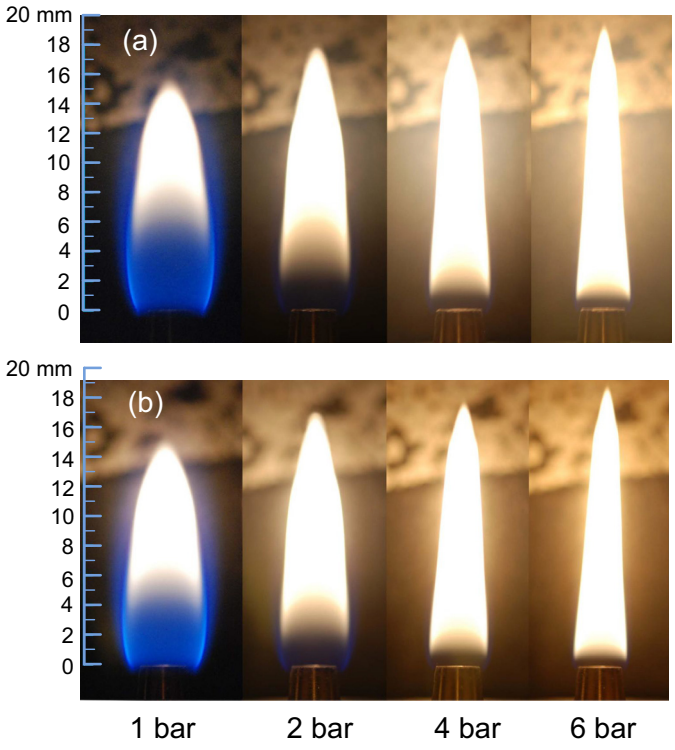

Fig. 2. Still pictures of the base fuel methane (a) and of the ethanol-doped methane (b) flames at various pressures.

3. Results and discussion

The geometric shape of the co-flow diffusion flame gets slimmer with increasing pressure such that the flame's radial cross-sectional area at a given height along the flame centerline shows an inverse proportionality to pressure [20,31]. Shapes of the flames of methane and ethanol-doped methane shown in Fig. 2 are very similar to the flames reported previously from high pressure experiments. The luminescent flame heights showed an increase of almost 10% from 2 bar to 6 bar, however the stoichiometric heights are expected to be invariant with pressure, see, e.g. [32]. Although the soot levels were very low in pure methane and ethanol-doped methane flames at atmospheric pressure, the increasing luminosity of the flames with increasing pressure indicate the soot concentrations are getting higher from 2 bar to 6 bar, Fig. 2. A qualitative comparison of the luminosities of the methane and ethanol-doped methane flames shows that in ethanol-doped flames the soot region, marked by yellow, appears slightly closer to the burner rim. (Fig. 2).

Soot volume fraction profiles of base methane and ethanol-doped methane flames at 2 bar pressure are displayed in Figs. 3

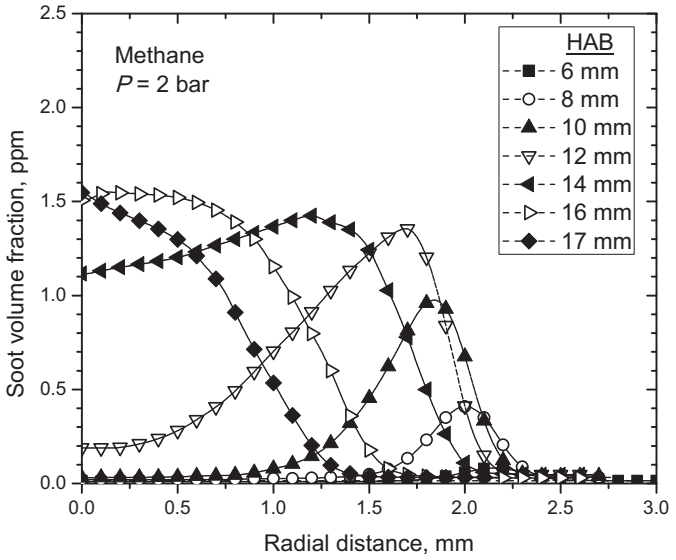

Fig. 3. Soot volume fraction profiles along the radial distance in base methane flame at 2 bar pressure. HAB represents the height above the burner exit along the flame centerline.

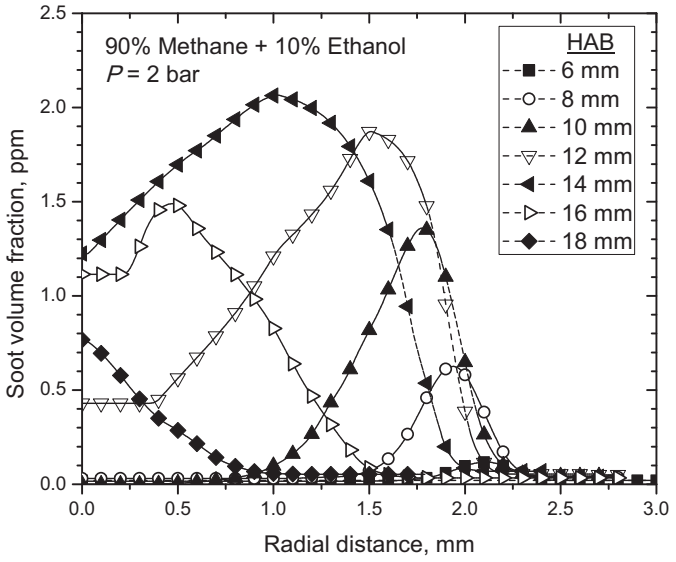

Fig. 4. Soot volume fraction profiles along the radial distance in ethanol-doped methane flame at 2 bar pressure. HAB represents the height above the burner exit along the flame centerline.

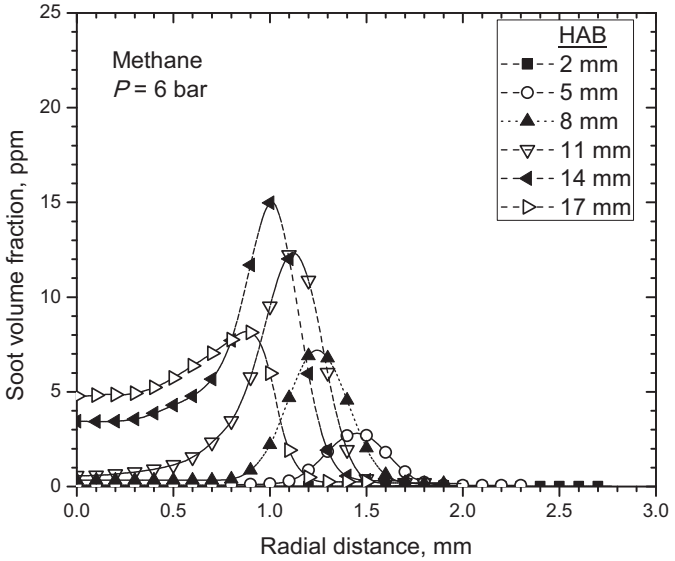

Fig. 5. Soot volume fraction profiles along the radial distance in base methane flame at 6 bar pressure. HAB represents the height above the burner exit along the flame centerline.

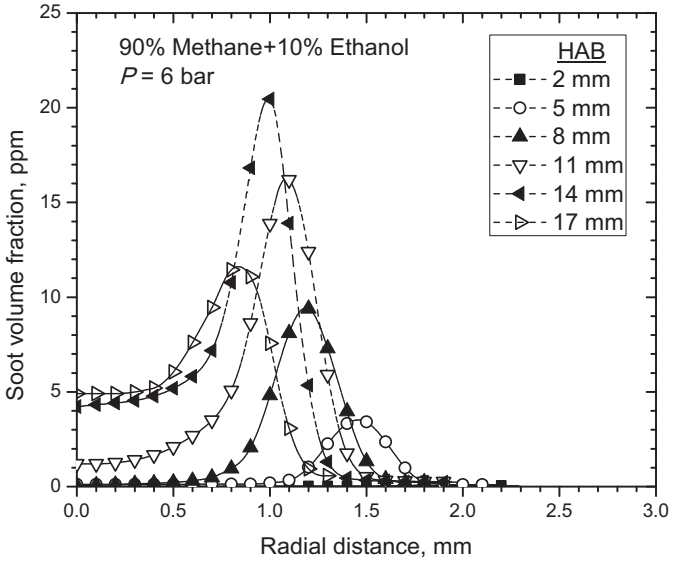

Fig. 6. Soot volume fraction profiles along the radial distance in ethanol-doped methane flame at 6 bar pressure. HAB represents the height above the burner exit along the flame centerline.

and 4, respectively, at various heights above the burner exit to provide a quantitative comparison. The general appearance of the radial soot volume fraction distributions at various heights is typical of laminar co-flow diffusion flames; maximum soot appears at a radial distance from the flame centerline at lower heights and it moves towards the centreline with increasing height. At all heights above the burner exit, ethanol-doped methane flame display higher soot volume fractions than the base methane flame up to about 30%. In base methane flame, the maximum soot volume fraction is about 1.6 ppm at a height of 16 mm, whereas in ethanol-doped methane flame maximum soot is 2.1 ppm at a height of 14 mm, Figs. 3 and 4. At 6 bar pressure, maximum soot volume fractions show an almost ten fold increase as compared to 2 bar results, Figs. 5 and 6. Maximum soot volume fractions are observed at the height of 14 mm in both flames; it is about 15 ppm in the base methane flame and just over 20 ppm in ethanol-doped methane flame, Figs. 5 and 6.

Comparing the radial soot profiles depicted in Figs. 5 and 6, one can notice that soot volume fractions at the lower heights and along the flame centerline are similar in undoped and ethanol-doped flames. Major differences seem to be limited to a radial ring around the flame centerline with radius from 0.5 to 1.2 mm. This implies that ethanol addition to methane influences mainly the soot growth region of the flame.

To have an overall picture of the comparison of the two flames from atmospheric to 6 bar, maximum soot volume fractions are depicted as a function of pressure in Fig. 7 on logarithmic scales. Influence of 10% carbon from ethanol in methane on soot volume fractions is displayed in Fig. 7. In the pressure range considered in this work, ethanol-doped methane flames produced consistently higher maximum soot concentrations than base methane flames.

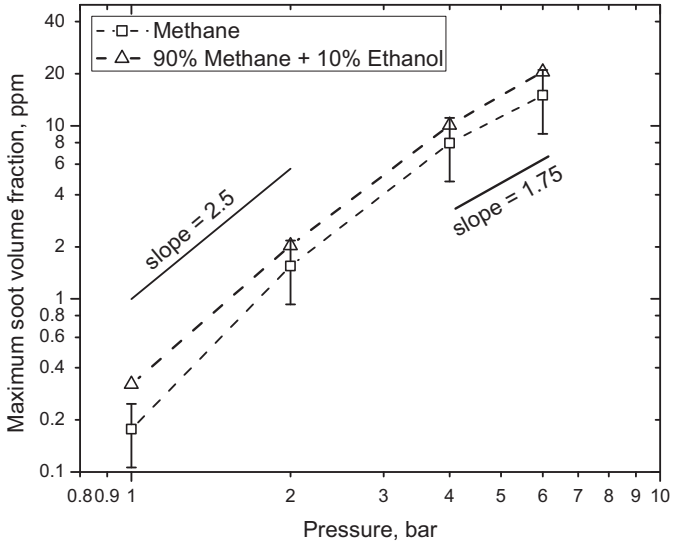

Fig. 7. Comparison of the maximum soot volume fraction of the base methane and ethanol-doped methane flames at various pressures on a logarithmic plot.

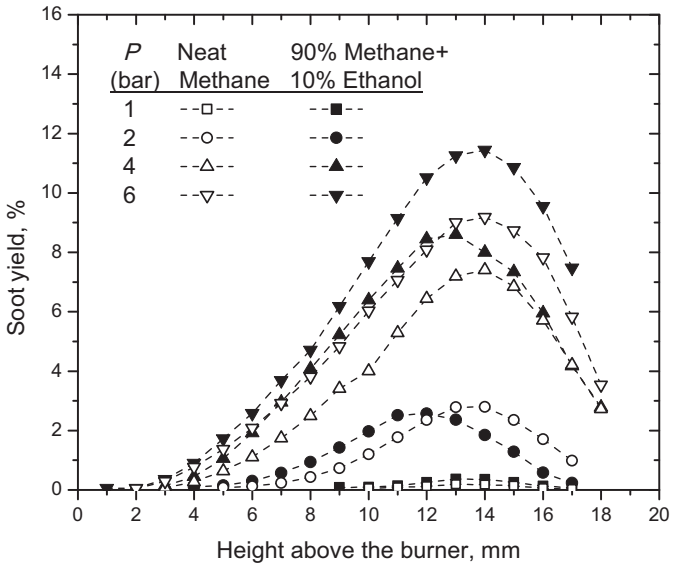

Fig. 8. Soot yield profiles of methane and ethanol-doped methane flames at various pressures as a function of the height above the burner exit. Percentages reflect the percentage of carbon from each fuel.

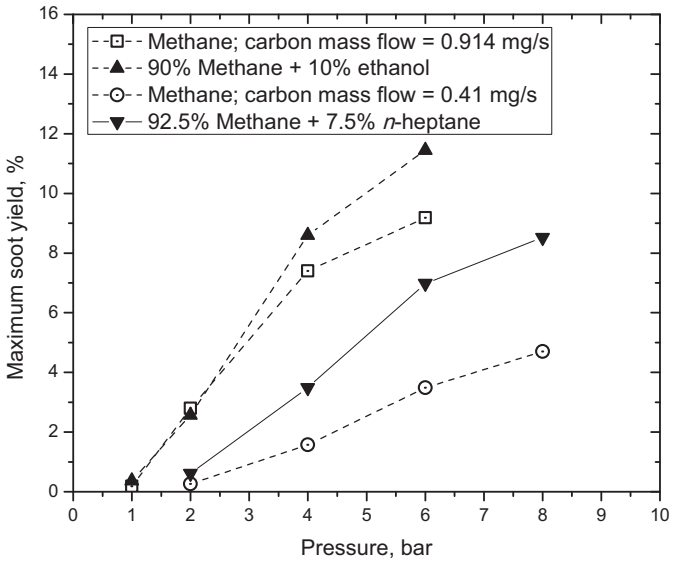

Fig. 9. Maximum soot yields of methane and ethanol-doped methane flames at various pressures. Also shown for comparison are the maximum soot yields of methane and *n*-heptane-doped methane flames taken from [34]. Percentages reflect the percentage of carbon from each fuel.

To provide visual help in assessing the sensitivity of the maximum soot volume fractions to pressure, reference slopes for guidance are included in the plot, Fig. 7. Variation of the maximum soot volume fraction with pressure in methane flames is similar to those in ethane [20] and propane flames [33] when scaled appropriately [22]. With the addition of ethanol to methane the pressure sensitivity of the maximum soot volume fraction did not show any significant change, Fig. 7. In a previous study, liquid fuels *n*-heptane or toluene were added to methane, such that 7.5% carbon was from the liquid fuel. The pressure sensitivity of the *n*-heptane-doped methane flame was similar to that of the neat methane flame, whereas the toluene-doped methane flame displayed a relatively weaker dependence on pressure [34].

When pressure is changed, the volume of the flame gas is compressed accordingly whereas the soot volume is not affected; as a consequence, soot volume fraction may not be a good metric to assess the influence of pressure. The common practice is to use soot yield as an indicator to evaluate the pressure dependence of soot processes. Soot yield represents the fraction of the fuel's carbon observed as soot at a given location within the flame envelope. The definition of the soot yield assumes that measured soot consists of carbon only. At a given axial cross section along the flame axis, one can estimate the mass flow of soot, $\dot{m}_s$, if the velocity field and the radial distribution of the soot volume fraction at that cross section are known, i.e.,

$$\dot{m}_s(z) = \rho_s \int 2\pi r f_v(r,z) v(r,z) \mathrm{d}r \tag{1}$$

In Eq. (1), ρ_s is the soot density, f_v is the soot volume fraction, v is the velocity, and r and z are the radial and axial coordinates, respectively. Eq. (1) assumes that the density of soot is constant within the flame envelope. We took the soot density as 1.8 g/cm^3 to have comparable data with our previous studies [19,29]. Detailed numerical simulations of co-flow laminar diffusion flames at pressure showed that it is possible to represent the velocity field by $(2az)^{1/2}$, in which a is a buoyancy-driven acceleration which can be approximated by $a \approx$ 41 m/s^2 and the further details can be found in [32,35]. Then, one can estimate the soot yield, Y_s, from

$$Y_s = \dot{m}_s(z)/\dot{m}_c \tag{2}$$

where $\dot{m}_c$ is the mass flow of carbon in the fuel at the burner exit. Mass flow rate of carbon was kept constant as 0.914 mg/s in this study. Eqs. (1) and (2) were used to infer the soot yields from soot volume fraction distributions and the results are plotted in Fig. 8 for the two flames at various pressures along the height above the burner. Ethanol-doped methane flame displays slightly higher soot yields at 1 bar, and at 2 bar both flames seem to produce similar soot yields; however at 4 and 6 bar, ethanol-doped methane flames display higher soot yields. It is apparent in Fig. 8 that maximum soot yield location moves slightly upstream in ethanol-doped methane flames.

To have a direct comparison, maximum soot yields from the data given in Fig. 8 are replotted in Fig. 9. The maximum soot yields of methane and ethanol-doped methane flames indicate that at 2 bar maximum soot yields are almost the same, except that maximum soot yield is realized earlier in ethanol-doped flames, as depicted in Fig. 8. Soot concentrations are relatively low at 1 bar pushing the limits of soot spectral emission technique, therefore

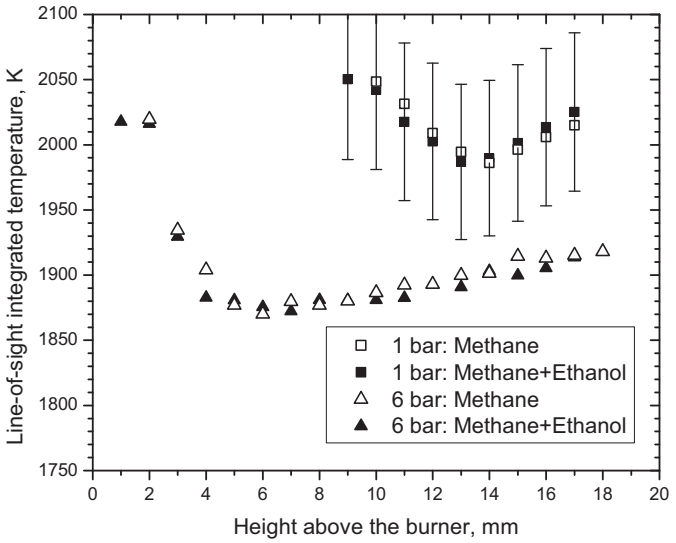

Fig. 10. Soot temperatures in methane and ethanol-doped methane flames at 1 and 6 bar pressures along the flame axis. Temperatures represent line-of-sight averaged values across the corresponding flame diameter.

the errors involved are the largest and the 1 bar results should be treated with caution. At 4 and 6 bar pressure flames, maximum soot yields of ethanol-doped methane flames are higher by about 16% and 25%, respectively, than those of neat methane flames, Fig. 9. Also plotted in Fig. 9 are the maximum soot yields of methane and *n*-heptane-doped methane flames adopted from [34]. A direct comparison of results from [34] to the current study may not be possible since the fuel flow rates are not the same. However, a qualitative comparison reveals that *n*-heptane addition to methane increases soot much more than ethanol addition.

The apparent inconsistency between the trends observed in Figs. 7 and 9 can be explained by considering the definition of the soot yield, Eq. 1. Maximum soot volume fraction is a local quantity whereas maximum soot yield represents integrated soot volume fraction across the flame radius at the height above the burner where it peaks. This means that two flames with identical maximum soot volume fractions could have very different maximum soot yields if the radial soot volume fraction distributions are not the same.

Salamanca et al. [36] observed a slowdown of soot formation and growth upon addition of ethanol in rich premixed flames of ethylene. In contrast, in diffusion flames of ethanol-doped methane soot formation and growth show an enhancement, especially at higher pressures.

Line-of-sight averaged flame temperatures, obtained by integrating the radially resolved temperatures over the flame diameter, are shown in Fig. 10 along the flame centerline at 1 and 6 bar. It is clear from Fig. 10 that the line-of-sight averaged flame temperatures of both flames are almost identical at a given pressure. Since the flame temperature of ethanol is expected to be about 20–25 K higher than that of methane under the same initial conditions, with the addition of ethanol to methane, to replace 10% of the methane's carbon with ethanol carbon, would increase the flame temperature of ethanol-doped methane by a few degrees. On the other hand, relatively higher soot loading of ethanol-doped methane flame would experience a slightly higher heat loss from the flame as a consequence of soot radiation. These two effects, higher flame temperature of ethanol and relatively higher radiative heat loss from ethanol-doped flame, seem to cancel each other leading to the very similar temperature profiles shown in Fig. 10. This ensures that, to a first approximation, at a given pressure the effect of any temperature difference on the soot processes in the two flames considered here could be neglected.

In the fuel decomposition of the ethanol-doped methane flames, the ethanol component of the fuel stream is expected to decompose earlier at a relatively lower temperature than methane. The main decomposition products of ethanol in a shock tube study were identified as C_2H_4, CH_3, CHO, CH_4, and C_2H_2, in addition to ethanol and water [37]. In a similar shock tube investigation [38], it was found that the major pyrolysis products of ethanol are water and C_2H_4; most of the observed C_2H_2 is argued to be produced from C_2H_4 via subsequent reactions. Previous studies that showed synergystic effects pointed to production of CH_3 from ethanol pyrolysis in ethanol-doped ethylene flames [9], and C_2H_2 production in pyrolysis of ethanol–toluene mixtures [16]. Current experimental results are not amenable to pass judgement whether there is a synergystic effect involved in ethanol-doped methane diffusion flames mainly due to the unavailability of reference soot data with neat ethanol. Production of CH_3 and C_2H_2 as some of the decomposition products of ethanol could be suspected to lead to some synergistic effects; however, methane itself decomposes to CH_3 and C_2H_2 [39], among other species, although at a relatively higher temperature than ethanol, which may not lead to any synergy [9].

The maximum uncertainty in inferring the temperatures from the spectral radiation measurements was evaluated as 3.5%. The maximum total uncertainty in soot measurements was estimated as 40%.These maximum uncertainties are shown in Figs. 7 and 10 as error bars. In our previous studies using the same diagnostics and analysis methods with various fuels at high pressures, the estimated maximum uncertainties were similar to current ones [19,20,23,25,29,33]. It should be noted that a significant portion of the evaluated uncertainties results from systematic errors. The main component of the systematic errors in this case is the uncertainty in the soot refractive index which would account for 70–80% of the total uncertainties in soot and temperature measurements. Systematic errors skew the data in one direction, mostly by a scale factor; hence the observed trends in comparisons of the data are not affected by the systematic errors. Consequently, the uncertainties originating from random errors are relatively small and the data trends observed in this study are statistically sound. As a result, conclusions reached from the presented results are reliable. For consistency, we used the same soot refractive index as in our previous high pressure soot studies [20,29], and the soot refractive index function was taken as 0.27. The details of the uncertainty analysis methodologies adopted in this work are available in studies reported previously [28,40].

4. Conclusions

Effect of ethanol blending on soot production was investigated in coflow laminar diffusion flames stabilized at pressures from atmospheric to 6 bar in a constant volume combustion chamber. The chamber and the co-flow laminar diffusion flame burner had been used before for measurements of soot and temperature in high pressure flames. Base fuel was methane and ethanol was blended to methane such that 10% of the carbon in the fuel stream would originate from the ethanol. Mass flow rate of carbon in the fuel streams was kept constant at 0.942 mg/s for base methane and ethonol-doped methane flames so that the measured data could be compared for the assessment of pressure dependence of soot. Luminescent flame heights showed about 10% change from 2 to 6 bar, excepting for the atmospheric ones, however, the stoichiometric flame heights are expected to be invariant ensuring almost constant flame residence times. Assuming axisymmetry, line-of-sight data of soot spectral radiation were inverted through an Abel algorithm to infer the radial temperature profiles at 1 mm inter-

vals along the flame axis. From the temperature data soot volume fractions, soot yields, and line-of-sight averaged soot temperatures were derived for methane and ethanol-doped methane flames at 1, 2, 4, and 6 bar. Ethanol-doped methane flames displayed higher soot concentrations than those of neat methane flames at all pressures considered in the study; however, pressure dependence of maximum soot volume fraction is almost the same for both neat methane and ethanol-doped methane. The results showed that the maximum soot volume fractions scale with pressure as P^n, where n decreases from about 2.5 to 1.8 from atmospheric to 6 bar which are similar pressure exponents to those reported previously for gaseous paraffinic fuels. A comparison of the maximum soot yields indicated that at lower pressures the two flames show a similar behaviour, however, at 4 and 6 bar pressure flames, maximum soot yields of ethanol-doped methane flames are higher by about 16% and 25%, respectively, than those of neat methane flames. A qualitative comparison to the soot yield of flames of methane doped with n-heptane showed that the increase in soot yield of ethanol-doped methane flames was relatively smaller. Since ethanol is being used widely in various countries as a fuel additive or extender, a better description of its sooting characteristics is desirable. Further high-pressure experimental studies with ethanol-doped hydrocarbon flames, complemented by numerical modelling, are required to bring a better insight into the pressure sensitivity of ethanol's sooting propensity, and extent of any synergistic effects.

Acknowledgments

The authors thank the Natural Sciences and Engineering Research Council of Canada for a discovery grant (RGPIN-2017-06063) and the Ontario Research Fund for a Research Excellence Program grant (ORF RE07-034), awarded to the senior author, for the support of this research work.

References

[1] V.H. Sachsse, E. Bartholemé, Beiträge zur frage der flammengeschwindigkeit, Z. Elektrochem. 53 (1949) 183–190.
[2] G.J. Gibbs, H.F. Calcote, Effect of molecular structure on burning velocity, J. Chem. Eng. Data 4 (1959) 226–237.
[3] Ö.L. Gülder, Burning velocities of ethanol-isooctane blends, Combust. Flame 56 (1984) 261–268.
[4] J. Li, A. Kazakov, F.L. Dryer, Ethanol pyrolysis experiments in a variable pressure flow reactor, Int. J. Chem. Kinet. 33 (12) (2001) 859–867.
[5] R. Selser, S. Humer, K. Seshadri, E. Pucher, Experimental investigation of methanol and ethanol flames in nonuniform flows, Proc. Combust. Inst. 31 (1) (2007) 1173–1180.
[6] B. Urban, K. Kroenlein, A. Kazakov, F. Dryer, A. Yozgatligil, M. Choi, S. Manzello, K. Lee, R. Dobashi, Sooting behavior of ethanol droplet combustion at elevated pressures under microgravity conditions, Microgravity Sci. Technol. 15 (3) (2004) 12–18.
[7] K. McNesby, A. Miziolek, T. Nguyen, F. Delucia, R. Skaggs, T. Litzinger, Experimental and computational studies of oxidizer and fuel side addition of ethanol to opposed flow air/ethylene flames, Combust. Flame 142 (4) (2005) 413–427.
[8] J. Wu, K. Song, T. Litzinger, S. Lee, R. Santoro, M. Linevsky, M. Colket, D. Liscinsky, Reduction of PAH and soot in premixed ethylene-air flames by addition of ethanol, Combust. Flame 144 (4) (2006) 675–687.
[9] C.S. McEnally, L.D. Pfefferle, The effects of dimethyl ether and ethanol on benzene and soot formation in ethylene nonpremixed flames, Proc. Combust. Inst. 31 (1) (2007) 603–610.
[10] M. Salamanca, M. Sirignano, A. D'Anna, Particulate formation in premixed and counter-flow diffusion ethylene/ethanol flames, Energy Fuels 26 (10) (2012) 6144–6152.
[11] M.M. Maricq, Soot formation in ethanol/gasoline fuel blend diffusion flames, Combust. Flame 159 (1) (2012) 170–180.
[12] A. Khosousi, F. Liu, S.B. Dworkin, N. A.Eaves, M. J.Thomson, X. He, Y. Dai, Y. Gao, F. Liu, S. Shuai, J. Wang, Experimental and numerical study of soot formation in laminar coflow diffusion flames of gasoline/ethanol blends, Combust. Flame 162 (2015) 2925–3933.
[13] Ö.L. Gülder, Influence of hydrocarbon fuel structural constitution and flame temperature on soot formation in laminar diffusion flames, Combust. Flame 78 (1989) 179–194.
[14] P.C. StJohn, P. Kairys, D.D. Das, C.S. McEnally, L.D. Pfefferle, D.J. Robichaud, M.R. Nimlos, B.T. Zigler, R.L. McCormick, T.D. Foust, Y.J. Bomble, S. Kim, A quantitative model for the prediction of sooting tendency from molecular structure, Energy Fuels 31 (2017) 9983–9990.
[15] M. Frenklach, J. Yuan, Effect of alcohol addition on shock-initiated formation of soot from benzene, International Symposium on Shock Tubes and Waves 16 (1987) 467–471.
[16] A. Alexiou, A. Williams, Soot formation in shock-tube pyrolysis of toluene, toluene-methanol, toluene-ethanol and toluene-oxygen mixtures, Combust. Flame 104 (1996) 51–65.
[17] M. Storch, M. Koegl, M. Altenhoff, S. Will, L. Zigan, Investigation of soot formation of spark-ignited ethanol-blended gasoline sprays with single- and multi–component base fuels, Appl. Energy 181 (2016) 278–287.
[18] C. Kim, F. Xu, G. Faeth, Soot surface growth and oxidation at pressures up to 8.0 atm in laminar nonpremixed and partially premixed flames, Combust. Flame 152 (2008) 301–316.
[19] H.I. Joo, Ö.L. Gülder, Soot formation and temperature field structure in co-flow laminar diffusion flames at pressures from 10 to 60 atmospheres, Proc. Combust. Inst. 32 (2009) 769–775.
[20] P.M. Mandatori, Ö.L. Gülder, Soot formation in laminar ethane diffusion flames at pressures from 0.2 to 3.3 MPa, Proc. Combust. Inst. 33 (2011) 577–584.
[21] M. Commodo, P.H. Joo, G. De Falco, P. Minutolo, A. D'Anna, Ö.L. Gülder, Raman spectroscopy of soot sampled in high-pressure diffusion flames, Energy Fuels 31 (2017) 10158–10164.
[22] Ö.L. Gülder, G. Intasopa, H.I. Joo, P.M. Mandatori, D.S. Bento, M.E. Vaillancourt, Unified behaviour of maximum soot yields of methane, ethane, and propane laminar diffusion flames at high pressures, Combust. Flame 158 (2011) 2037–2044.
[23] H. Joo, Ö.L. Gülder, Experimental study of soot and temperature field structure of laminar co-flow ethylene–air diffusion flames with nitrogen dilution at elevated pressures, Combust. Flame 158 (2011) 416–422.
[24] P.H. Joo, Ö.L. Gülder, Formation of liquid methane water mixture during combustion of a laminar methane jet at supercritical pressures, Energy Fuels 26 (2012) 5462–5467.
[25] A.E. Karatas, G. Intasopa, Ö.L. Gülder, Sooting behaviour of n-heptane laminar diffusion flames at high pressures, Combust. Flame 160 (2013) 1650–1656.
[26] P.H. Joo, M.R.J. Charest, C.P.T. Groth, Ö.L. Gülder, Comparison of structures of laminar methane–oxygen and methane–air diffusion flames from atmospheric to 60 atm, Combust. Flame 160 (2013) 1990–1998.
[27] F. Liu, A.E. Karataş, Ö.L. Gülder, M. Gu, Numerical and experimental study of the influence of CO_2 and N_2 dilution on soot formation in laminar coflow C_2H_4/air diffusion flames at pressures between 5 and 20 atm, Combust. Flame 162 (2015) 2231–2247.
[28] D. Snelling, K. Thompson, G. Smallwood, Ö.L. Gülder, Spectrally resolved measurement of flame radiation to determine soot temperature and concentration, AAIA J. 40 (9) (2002) 1789–1795.
[29] K.A. Thomson, Ö.L. Gülder, R.A. Weckman, E.J. Fraser, G.J. Smallwood, D.R. Snelling, Soot concentration and temperature measurements in co-annular, nonpremixed CH_4/air laminar diffusion flames at pressures up to 4 MPa, Combust. Flame 140 (2005) 222–232.
[30] M.R.J. Charest, H. Joo, C.P.T. Groth, Ö.L. Gülder, A numerical study on the effects of pressure and gravity in laminar ethylene diffusion flames, Proc. Combust. Inst. 33 (2011) 549–557.
[31] A.E. Karataş, Ö.L. Gülder, Soot formation in high pressure laminar diffusion flames, Progr. Energy Combust. Sci. 38 (2012) 818–845.
[32] M.R.J. Charest, C.P.T. Groth, Ö.L. Gülder, A numerical study on the effects of pressure and gravity in laminar ethylene diffusion flames, Combust. Flame 158 (2011) 1933–1945.
[33] D.S. Bento, K.A. Thomson, Ö.L. Gülder, Soot formation and temperature field structure in laminar propane-air diffusion flames at elevated pressures, Combust. Flame 145 (2006) 765–778.
[34] A.E. Daca, O.L. Gülder, Soot formation characteristics of diffusion flames of methane doped with toluene and n-heptane at elevated pressures, Proc. Combust. Inst. 36 (2017) 737–744.
[35] Ö.L. Gülder, Corrigendum to dependence of sooting characteristics and temperature field of co-flow laminar pure and nitrogen-diluted ethyleneair diffusion flames on pressure, Combust. Flame 173 (2017) 1.
[36] M. Salamanca, M. Sirignano, M. Commodo, P. Minutolo, A. D'Anna, The effect of ethanol on the particle size distributions in ethylene premixed flames, Exp. Thermal Fluid Sci. 43 (2012) 71–75.
[37] M. Aghsaee, D. Nativel, M. Bozkurt, M. Fikri, N. Chaumeix, C. Schulz, Experimental study of the kinetics of ethanol pyrolysis and oxidation behind reflected shock waves and in laminar flames, Proc. Combust. Inst. 35 (2015) 393–400.
[38] J. Kiecherer, C. Bänsch, T. Bentz, M. Olzmann, Pyrolysis of ethanol: a shock–tube/TOF-MS and modeling study, Proc. Combust. Inst. 35 (2015) 465–472.
[39] G.L. Agafonov, A.A. Borisov, V.N. Smirnov, K.Y. Troshin, P.A. Vlasov, J. Warnatz, Soot formation during pyrolysis of methane and rich methane/oxygen mixtures behind reflected shock waves, Combust. Sci. Technol. 180 (10–11) (2008) 1876–1899.
[40] K.A. Thomson, Soot formation in annular non-premixed laminar flames of methane–air at pressures of 0.1–4.0 MPa, University of Waterloo, 2004 Ph.D. thesis.